



Supplementary Information for

Directional Pumping of Water and Oil Microdroplets on Slippery Surface

Jieke Jiang, Jun Gao, Hengdi Zhang, Wenqing He, Jianqiang Zhang, Dan Daniel and Xi Yao

Xi Yao

Email: xi.yao@cityu.edu.hk

This PDF file includes:

Supplementary experimental details
Figs. S1 to S11
Tables S1
Captions for movies S1 to S3
References for SI reference citations

Other supplementary materials for this manuscript include the following:

Movies S1 to S3

Supplementary Experimental Details

Spraying microdroplets. A thin film chromatography sprayer (250 mL, Sigma Aldrich) was used to generate the microdroplets. The gas flow of compressed air was generated by squeezing the rubber pump of the sprayer with a customized actuator. The distance between the sprayer and the sample was set at 15 cm.

Generation of single microdroplets. A steel needle with flat top and inner diameter of 60 μm was used to fabricate a superhydrophobic needle. The needle was immersed into a solution formulated by dissolving 1 g fumed silica (22 nm, Sigma-Aldrich) and 1 g PDMS precursor (10: 1 base and curing agent) in 15 ml n-hexane for several times to overcoat a superhydrophobic layer on the needle. By using the superhydrophobic needle, the squeezed microdroplets will not adhere on the tip of the needle, which can facilitate the control of the droplet diameter. The superhydrophobic needle was mounted on a three-dimensional mobile platform with a universal joint. A microliter syringe (500 μL , Hamilton) filled with deionized water was connect with the needle by a plastic tubing. The volume of the droplet generated by the needle was controlled by a syringe pump (KDS 100, KDS Scientific). For the generation of tiny oil droplet, the FC-70 and olive oil will adhere on the needle due to their low surface tension. However, those oil droplets were still able to detach from the needle when contact with the slippery surface because of the low surface tension of the superhydrophobic needle.

Confocal microscope imaging of the oil meniscus. The cross section of the oil meniscus was imaged using Zeiss LSM 880 laser confocal microscope. The solid PDMS was stained with Nile red (J & K Scientific) by a swelling method. Nile red was dissolved in ethanol to form a 200 mM solution. 100 μL of this solution was dispensed into 20 mL silicone oil. The as-prepared silicone oil was used to swell a solid PDMS for 5 hours. Then, the lubricant layer on the surface was thoroughly washed by pure silicone oil without dye. Then the surface was carefully wiped by a filter paper. Silicone oil stained with coumarin-6 (J & K Scientific) prepared by the same procedure

was used to form the lubricant layer. Certain volume of silicone oil stained with coumarin-6 was over-coated on the wiped surface with known area. The as prepared substrate was used for confocal characterization. After each capturing, a confocal Z-stacking mode was applied to visualize the cross section of the oil meniscus.

Preparation of bacterial medium. GFP-tagged *E. coli* and *Staphylococcus aureus* (*S. aureus*) without GFP-tag were used in the bacterial collection test and bactericidal test. The bacterial medium was prepared in the same manner which is described as following. A single colony of *E. coli* or *S. aureus* on a solid Luria-Bertani (LB) agar plate was transferred to 30 mL of liquid LB culture medium and was grown at 37°C for 12 hours. Bacteria were harvested by centrifugation (7100 rpm for 2 min), and then washed twice with sterilized phosphate-buffered saline (PBS) solution. The supernatant was discarded and the pellet was re-suspended in 30 ml sterilized PBS solution. This suspension of *E. coli* or *S. aureus* was used as the medium for generating bacteria-containing microdroplets. These microdroplets were sprayed on the testing surfaces and characterized with fluorescent microscope (Leica MZ10F Fluorescent Stereomicroscope). For the capturing of fluorescent images, the microscope was focused to the slippery surface at the bottom of the hydrogel dot under visible light. Then the microscope was switched to GFP channel to capture the driven process of bacteria. To measure the fluorescent signal of the collected bacteria, a rectangle covers the collected bacterial media on the hydrogel dot was chosen as the measuring area. The width of the rectangle equals to the diameter of the collected droplet while its length equals to 7 mm. The fluorescent intensity at different position of x-axis is obtained by calculating the average signal on y-axis.

Loading of biocide onto the Hydrogel Dots. A slippery surface with hydrogel dot array were immersed into 5 mM solution of thyme essential oil for seconds and was took out slowly. The biocide solution adhered on the hydrogel dots forming droplet array. Before testing, the substrate was allowed to dry at room temperature for 0.5 hour. The bacteria medium stained with bacterial

viability kit was sprayed to the surface and the substrate was subsequently sent for fluorescence microscope observation (Nikon Eclipse Ni-E Fluorescent Microscope).

LIVE/DEAD BacLight bacterial viability assay. For the bactericidal test, a LIVE/DEAD BacLight bacterial viability kit (L7007, Thermo Fisher Scientific) was used to assess the bacterial cell viability of the collected *E. coli* on the hydrogel dot. In this assay, the red-fluorescent nucleic acid staining agent propidium iodide, which only penetrates damaged cell membrane, was used to label dead bacterial cells. 3 μL of propidium iodide was added to 10 mL of above obtained *E. coli* medium at room temperature and was kept in the dark for 15 min before used as the spraying solution. In the detection of *S. aureus*, SYTO 9 from the kit was used to stain the nuclear acid of *S. aureus*. SYTO 9 green fluorescent nucleic acid stain has been shown to stain live and dead Gram-positive and Gram-negative bacteria. 3 μL of SYTO 9 was added to 10 mL of above obtained *S. aureus* medium at room temperature and was kept in the dark for 15 min before used as the spraying solution.

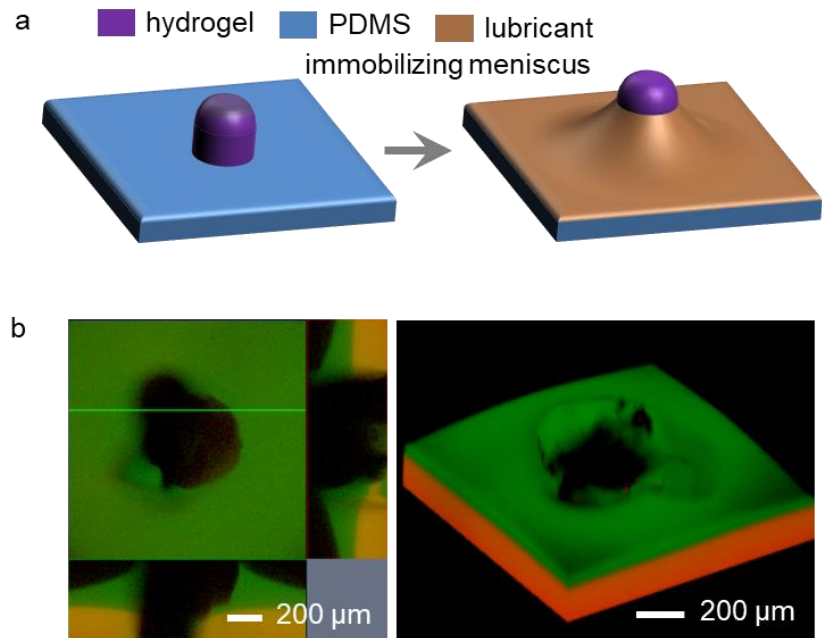


Fig. S1 Immobilized lubricant meniscus is formed around the surface-piercing hydrogel dot.
 (a) Scheme illustrating the formation of a lubricant meniscus around the hydrogel dot after adding lubricant to the patterned surface. (b) Confocal microscope images showing the formation of an oil meniscus around the hydrogel dot.

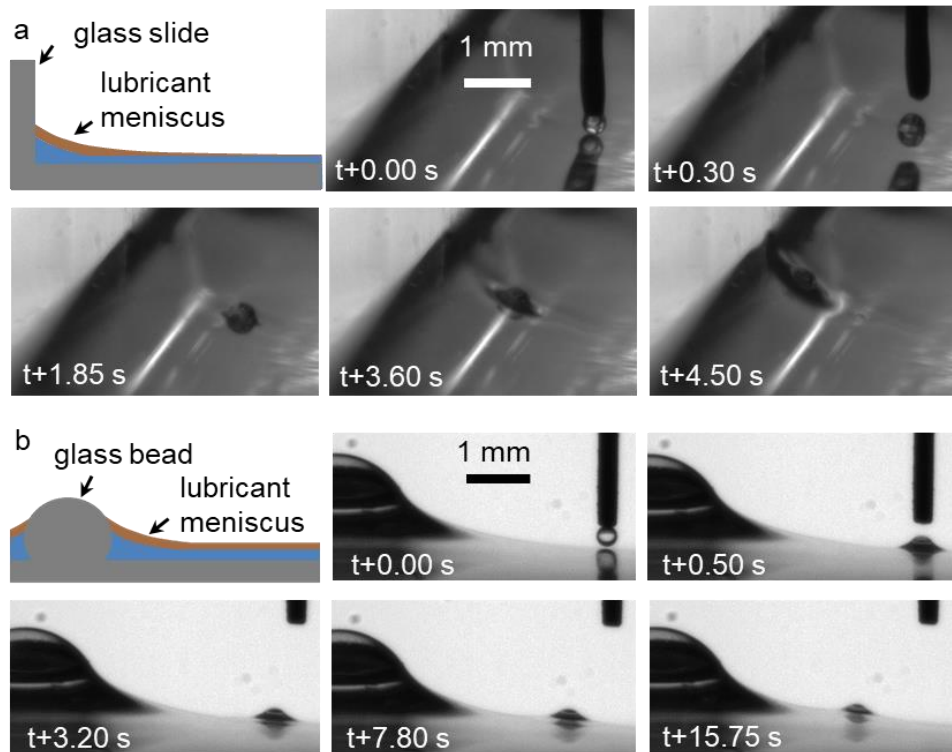


Fig. S2 Driven of water microdroplets by lubricant menisci immobilized by a vertical glass slide (a) and a glass bead (b). In both cases, the droplet could be driven by capillary pumping. The results indicate that the system is ubiquitous as long as a lubricant meniscus exists on the slippery surface. The glass bead and glass slide were washed by ethanol to be clean and hydrophilic.

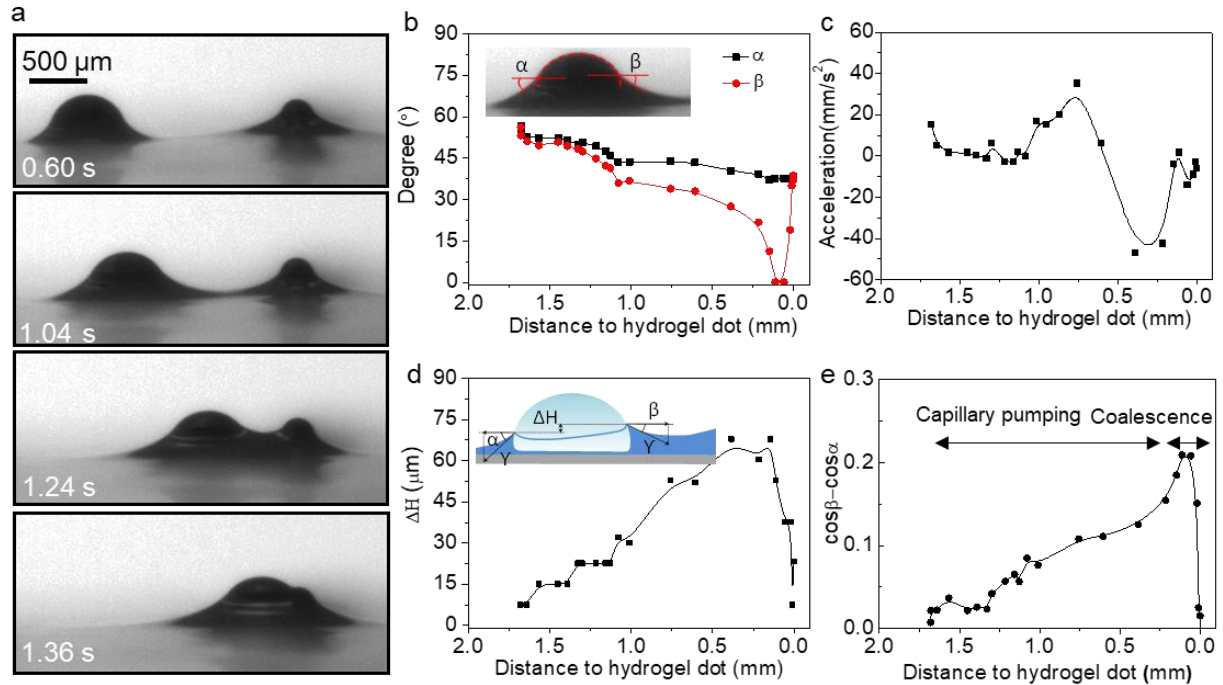


Fig. S3 A typical droplet driving process. (a) Time-lapsed microscope images showing a typical process to transport a microdroplet. The imbalance of lubricant wetting ridges increased as the droplet approaching the hydrogel dot. (b) The value of α and β of the microdroplet in the driving process in (a). (c) The calculated acceleration of the microdroplet in (a). (d) The height difference of the oil layer at the two opposite edges of the microdroplet in (a). (e) The value of $\cos\beta - \cos\alpha$ of the microdroplet as it was driven to the hydrogel dot in (a). $\cos\beta - \cos\alpha$ represents the capillary force, which increases with the decreasing of distance, qualitatively in agreement with the prediction that $F_c \propto \lambda/L$. Note that F_c is estimated to be in the order of 10^{-6} N, corresponding to an acceleration in the order of m/s^2 . This is dramatically larger than the values in (c), suggesting that the capillary force is indeed largely balanced by viscous drag force, as we discussed in the main text.

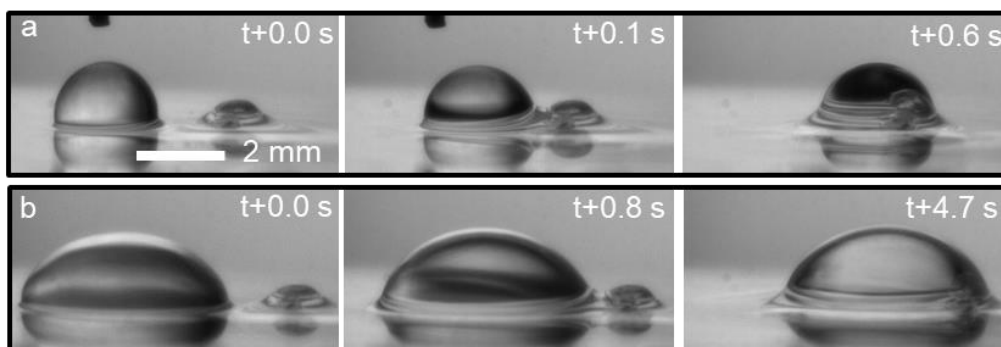


Figure S4 Successful driven of relatively large droplet by the capillary pumping system. Droplets with diameter of around 2 mm (a) and 5 mm (b) were driven to the hydrogel dot, respectively, demonstrates the driving system is also applicable for large droplets.

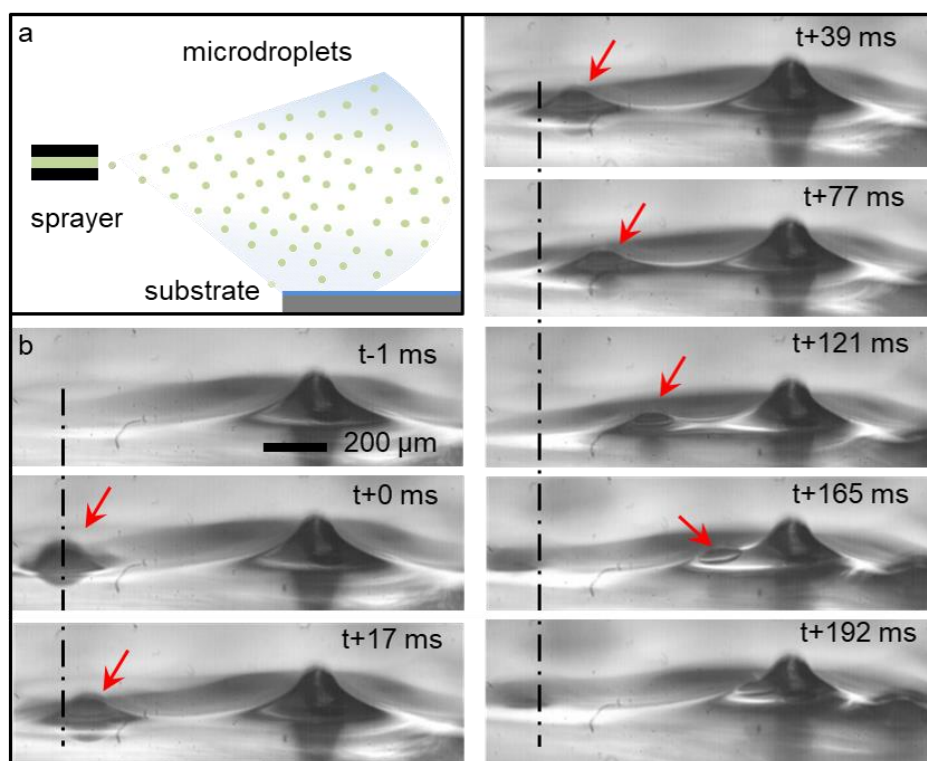


Fig. S5 Driven of an aerosolized tiny droplet with a diameter of $\sim 100 \mu\text{m}$. (a) Scheme showing the experimental setup. (b) Time-lapsed images captured by a high-speed camera showing a single aerosolized microdroplet with diameter of $\sim 100 \mu\text{m}$ was driven to the hydrogel dot.

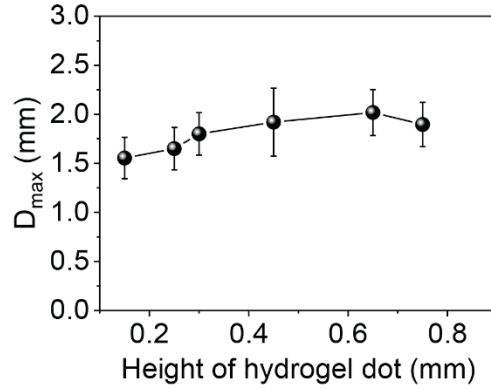


Fig. S6 Maximum driving distance D_{max} is relatively independent of hydrogel dot height.

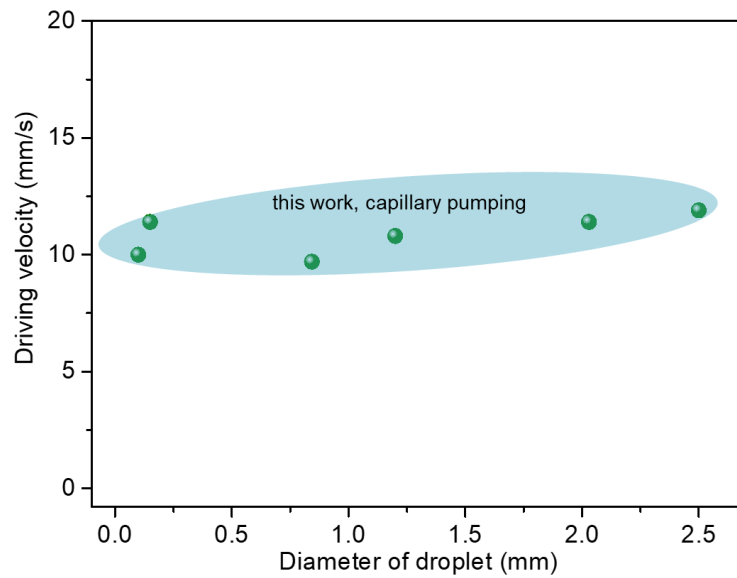


Fig. S7 Droplet diameter and highest driving velocity of our work. Our system is featured with driving of both water and oil microdroplets, driving droplets with a wide range of diameters, and driving droplet at a relatively high speed.

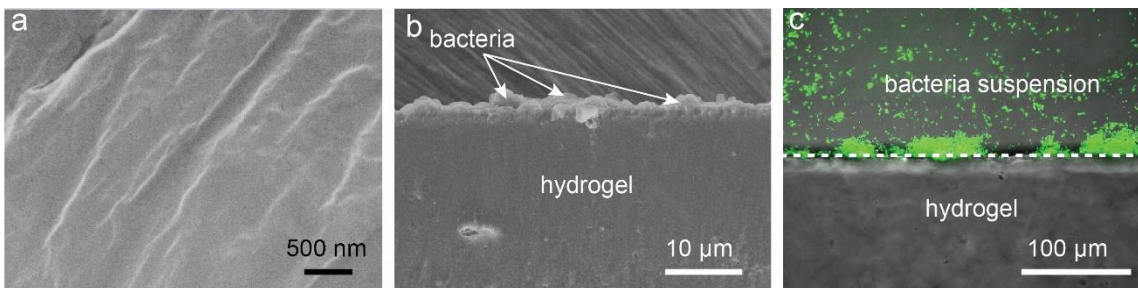


Fig. S8 Bacteria cannot enter hydrogel dot. (a) SEM image of hydrogel. No pores can be observed. The hydrogel is freeze-dried before SEM characterization to keep its microstructure. (b) SEM image of the bacteria on hydrogel, and (c) fluorescent image of bacteria suspension beside hydrogel (dashed line indicates hydrogel surface), showing that bacteria cannot enter hydrogel.

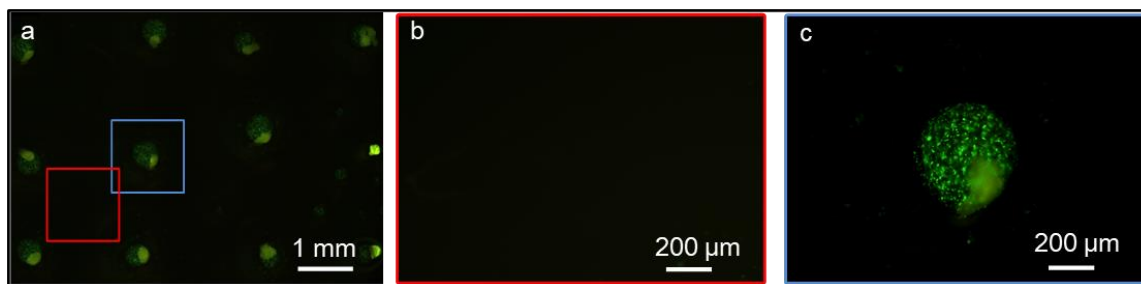


Fig. S9 Collection of aerosolized GFP-tagged *E. coli* by a 3×4 hydrogel dot array for multi-site enrichment and analysis. (a) Fluorescent microscope images showing the bacteria is successfully collected by the hydrogel dot array. Area outside the hydrogel dot keeps anti-fouling (b), while bacteria is collected to the hydrogel dot (c).

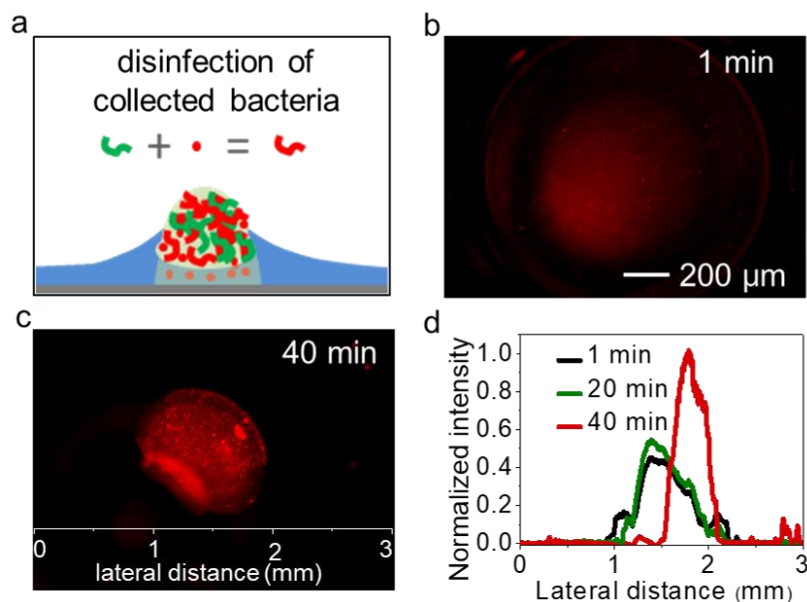


Fig. S10 Killing enriched bacteria via pre-immobilization of a biocide of thyme essential oil on the hydrogel dot. (a) A hydrogel dot loaded with thyme essential oil as biocide to disinfect collected bacteria. (b) and (c) Fluorescent microscope images showing the successful disinfection of collected bacteria. The red color indicates the dead bacteria stained with bacterial viability kit. (d) Measured fluorescent intensity at different time points of the disinfection process, suggesting the killing process.

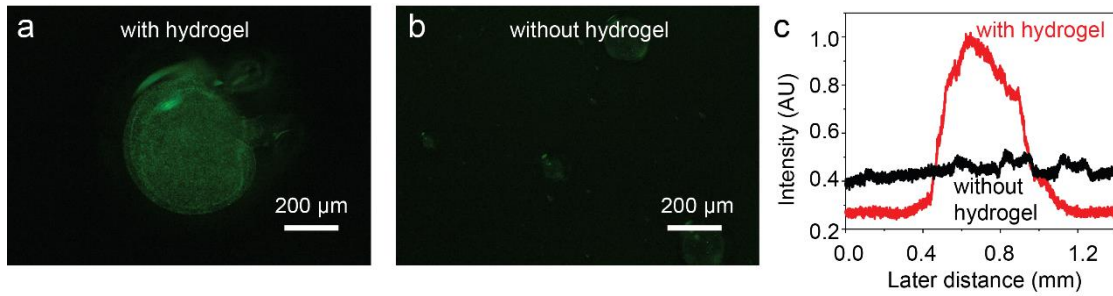


Fig. S11 Fluorescent microscope images showing *S. aureus* enriched by hydrogel dot. (a) Fluorescent image of hydrogel dot after the collection of *S. aureus*. The nucleic acid of *S. aureus* is stained by SYTO9 which is part of the LIVE/DEAD BacLight bacterial viability assay (Thermo Fisher). Strong fluorescence was observed on the hydrogel dot. (b) Fluorescent image of a planar slippery surface after the spray of bacteria. Only weak fluorescence signal was observed. (c) Average fluorescence intensity along the lateral dimension for (a) and (b).

Table S1 Comparison of the performance of this capillary pumping system with other droplet driving systems. Only our system is capable of driving both submillimeter-sized water and oil droplets.

	Driving strategy or system	Water/oil	Minimum droplet diameter (mm)	Reference	
Plenary surface	Surface-energy- gradient surface	Water	1.50	(1)	
		Water	2.30	(2)	
		Water	1.50	(3)	
		Water and oil	4.00	(4)	
		Water	2.00	(5)	
		Water	4.20	(6)	
	Structure-gradient surface	Water and oil	2.20	(7)	
		Water	1.90	(8)	
		Water	3.00	(9)	
		Water	1.50	(10)	
Curvature surface	Cone-shaped fiber (coalescence is needed to drive droplet)	Water	0.14	(11)	
		Water	0.02	(12)	
		Water	0.05	(13)	
		Water	0.15	(14)	
		Water	0.10	(15)	
		Oil	0.04	(16)	
	Slippery asymmetric bump (coalescence is needed to drive droplet)	Water	1.20	(17)	
		Microstructured lubricant-infused surface (coalescence is needed to drive the droplet)	Water	2.0	(18)
			Water	0.05	(19)
Capillary pumping on slippery surface		Water and oil	Minimum ~0.1 mm tested. Essentially there should be no limit.	This work	

Movie S1. Video showing a microdroplet being driven toward the hydrogel dot, bridged by the oil meniscus.

Movie S2. Video showing aerosol water droplets were sprayed onto the slippery surface with and without the surface-piercing hydrogel dot.

Movie S3. Video showing large-scale hydrogel dots array on the slippery collecting water microdroplets.

References

1. Daniel S, Chaudhury MK, & Chen JC (2001) Fast drop movements resulting from the phase change on a gradient surface. *Science* 291(5504):633-636.
2. Chaudhury MK & Whitesides GM (1992) How to Make Water Run Uphill. *Science* 256(5063):1539-1541.
3. Wang T, *et al.* (2018) Controlling Directional Liquid Motion on Micro-and Nanocrystalline Diamond/ β -SiC Composite Gradient Films. *Langmuir* 34(4):1419-1428.
4. Hernandez SC, *et al.* (2013) Chemical gradients on graphene to drive droplet motion. *ACS Nano* 7(6):4746-4755.
5. Ito Y, *et al.* (2007) The movement of a water droplet on a gradient surface prepared by photodegradation. *Langmuir* 23(4):1845-1850.
6. Banuprasad TN, *et al.* (2017) Fast transport of water droplets over a thermo-switchable surface using rewritable wettability gradient. *ACS applied materials & interfaces* 9(33):28046-28054.
7. Li J, *et al.* (2016) Oil droplet self-transportation on oleophobic surfaces. *Science Advances* 2(6):e1600148-e1600153.
8. Deng S, *et al.* (2017) Controlled droplet transport to target on a high adhesion surface with multi-gradients. *Scientific reports* 7:45687.
9. Wu H, *et al.* (2017) Smart design of wettability-patterned gradients on substrate-independent coated surfaces to control unidirectional spreading of droplets. *Soft matter* 13(16):2995-3002.
10. Bliznyuk O, Jansen HP, Kooij ES, Zandvliet HJ, & Poelsema B (2011) Smart design of stripe-patterned gradient surfaces to control droplet motion. *Langmuir* 27(17):11238-11245.
11. Ju J, *et al.* (2012) A multi-structural and multi-functional integrated fog collection system in cactus. *Nature Communications* 3:1247-1252.
12. Zheng Y, *et al.* (2010) Directional water collection on wetted spider silk. *Nature* 463(7281):640-643.
13. Bai H, *et al.* (2010) Direction Controlled Driving of Tiny Water Drops on Bioinspired Artificial Spider Silks. *Adv Mater* 22(48):5521-5525.
14. Bai H, *et al.* (2011) Large-Scale Fabrication of Bioinspired Fibers for Directional Water Collection. *Small* 7(24):3429-3433.
15. Ju J, Xiao K, Yao X, Bai H, & Jiang L (2013) Bioinspired Conical Copper Wire with Gradient Wettability for Continuous and Efficient Fog Collection. *Adv Mater* 25(41):5937-5942.
16. Li K, *et al.* (2013) Structured cone arrays for continuous and effective collection of micron-sized oil droplets from water. *Nature Communications* 4:2276-2282.
17. Park KC, *et al.* (2016) Condensation on slippery asymmetric bumps. *Nature* 531(7592):78-82.

18. Zheng YF, *et al.* (2017) Droplet Motion on a Shape Gradient Surface. *Langmuir* 33(17):4172-4177.
19. Kajiya T, *et al.* (2016) Cylindrical chains of water drops condensing on microstructured lubricant-infused surfaces. *Soft Matter* 12(46):9377-9382.